5420 J. Med. Chem. 2009, 52, 5420–5428
DOI: 10.1021/jm900559x

Journal of Medicinal Chemistry Article

Snapshots of the Fluorosalinosporamide/20S Complex Offer Mechanistic Insights for Fine Tuning Proteasome Inhibition†

Michael Groll,*,‡ Katherine A. McArthur,§ Venkat R. Macherla,§ Rama Rao Manam,§ and Barbara C. Potts*,§

‡Center for Integrated Protein Science at the Department of Chemistry, Lehrstuhl für Biochemie, Technische Universität München, Lichtenbergstrasse 4, Garching D-85747, Germany, and §Nereus Pharmaceuticals, Inc., 10480 Wateridge Circle, San Diego, California 92121

Received May 1, 2009

Many marketed drugs contain fluorine, reflecting its ability to modulate a variety of biological responses. The unique 20S proteasome inhibition profile of fluorosalinosporamide compared to chlorinated anticancer agent salinosporamide A (NPI-0052) is exemplary and relates to each halogen's leaving group potential. Crystal structures of fluoro-, hydroxy-, and bromosalinosporamide in complex with the yeast 20S proteasome core particle (CP) provide mechanistic insights into ligand binding and leaving group elimination and the ability to fine-tune the duration of proteasome inhibition. Fluorosalinosporamide/CP crystal structures determined over time offer striking snapshots of the ligand trapped with an intact fluoroethyl group in anticipation of fluoride elimination, followed by complete nucleophilic displacement of fluoride to give the highly stabilized cyclic ether found for salinosporamide A and bromosalinosporamide. This two-step reaction pathway is consistent with a mechanism for partially reversible proteasome inhibition by fluorosalinosporamide. Proteasome catalyzed fluoride displacement provides preliminary insights into the active site Thr1N pK_a.

Introduction

The 26S proteasome is a multicatalytic enzyme complex that is responsible for degradation of intracellular proteins and has emerged as a validated target for the treatment of cancer.[1,2] Downstream consequences of selective proteasome inhibition include blocking the activation of the NF-κB pathway, interfering with the timely degradation of cyclins and other proteins that regulate the cell cycle, and stabilizing proapoptotic proteins. These defined mechanisms of action supported the exploration of the therapeutic potential of proteasome inhibitors, and in 2003, the U.S. Food and Drug Administration approved bortezomib ((*R*)-3-methyl-1-((*S*)-3-phenyl-2-(pyrazine-2-carboxamido)propanamido)butylboronic acid) for the treatment of relapsed and/or refractory multiple myeloma, effectively validating the proteasome as a target in oncology.[3,4] "Lessons learned" from bench to bedside have been recently reviewed.[2] Predating clinical studies, proteasome structural biology provided an in-depth understanding of the structure and function of this complex molecular machine.[5] Proteolysis occurs within the 20S core particle (CP[a]), which comprises 28 subunits forming four stacked rings, together creating a barrel shaped structure with a central cavity through which protein substrates enter and peptide hydrolysis products exit.[6,7] The two central rings contain three pairs of proteolytic subunits (β5, β2, and β1) for which chymotrypsin-like (CT-L), trypsin-like (T-L), and caspase-like (C-L) activities have been respectively conferred on the basis of their substrate specificities. The proteolytic subunits are classified among the N-terminal nucleophile hydrolase family of enzymes in light of the active site architecture, which possesses an N-terminal nucleophilic threonine residue that catalyzes substrate hydrolysis.[6,7]

Understanding the details of 20S proteasome function has benefited from studies of the 20S CP in complex with a variety of inhibitors, including members of the β-lactone–γ-lactam family.[8−10] One such inhibitor is anticancer agent salinosporamide A (**1** (NPI-0052), Chart 1),[11,12] a chlorinated marine natural product that is active in several nonclinical tumor models[13−16] and is currently in clinical trials for the treatment of patients with hematologic and solid tumor malignancies.[12,14,17,18] A characteristic feature of **1** is its prolonged duration of inhibition of all three 20S proteolytic functions in vitro and in vivo,[13,19] with parallel observations in packed whole blood lysates obtained from patients in clinical trials.[20] We therefore sought to elucidate the mechanism of prolonged inhibition at the molecular level and embarked on a series of structure–activity relationship and structural biology studies.[19,21,22] Crystal structures of **1** and deschloro analogue **2** in complex with the yeast 20S CP revealed a unique binding mechanism for **1** in which covalent addition of Thr1O$^{\gamma}$ to the β-lactone carbonyl is followed by elimination of the chlorine leaving group (LG). We hypothesized that the resulting highly stabilized cyclic ether end product (Scheme 1, **Ib**′) renders **1** irreversibly bound.[22] These findings were supported by inhibition/recovery studies on a suite of analogues, which clearly demonstrated that the presence of

†Atomic coordinates for the hydroxysalinosporamide/20S proteasome CP complex have been assigned PDB code 3HYE. Coordinates for the fluorosalinosporamide/20S proteasome CP complexes have been assigned PDB codes 3GPT and 3GPW.

*To whom correspondence should be addressed. For M.G.: phone, +49-(0)89-289-13361; fax, +49-(0)89-289-13363; e-mail, michael.groll@ch.tum.de. For B.C.P.: phone, 858-587-4090; fax, 858-587-4088; e-mail, bpotts@nereuspharm.com.

[a] Abbreviations: CP, core particle; LG, leaving group; CT-L, chymotrypsin-like; T-L, trypsin-like; C-L, caspase-like; IC_{50}, concentration that results in 50% inhibition; EDTA, ethylenediaminetetraacetic acid; MES, morpholinoethanesulfonic acid; MPD, 2-methyl-2,4-pentanediol.

 Published on Web 08/13/2009

Chart 1

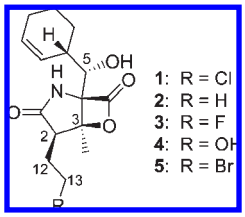

Scheme 1. Mechanism of Inhibition of the 20S Proteasome by LG and Non-LG Analogues and Potential Pathways for Recovery of Enzymatic Activity and Aqueous Hydrolysis[a]

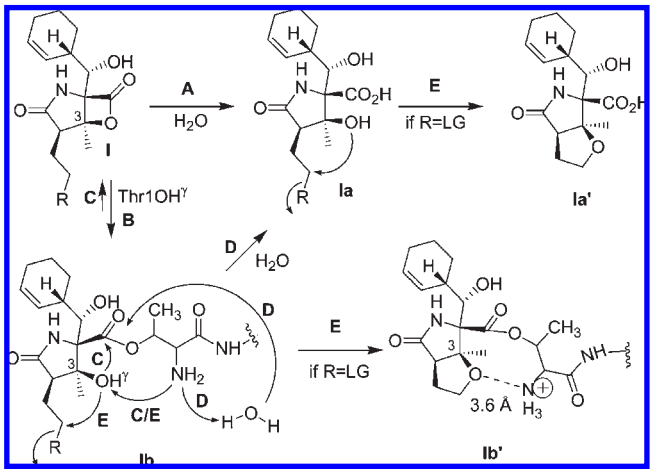

[a] Pathway A: aqueous hydrolysis of β-lactone in solution. B: ester formation between the inhibitor and Thr1O$^{\gamma}$. C: re-formation of the β-lactone within the proteasome active site. D: hydrolysis of the inhibitor−Thr1O$^{\gamma}$ ester bond. E: intramolecular nucleophilic displacement (pathway only active when R = LG).

a good LG imparts prolonged duration inhibition of isolated proteasomes in vitro. Those analogues bearing LGs (giving rise to **Ib′**) were classified as irreversible inhibitors, while non-LG analogues acted as slow substrates.[19]

The differences in the biological activities of **1** and **2**, bearing chlorine and hydrogen, respectively, begged the question of the behavior of a fluorinated analogue. Fluorine is frequently introduced into medicinal compounds to modulate a variety of biological responses ranging from pharmacokinetics to ligand binding affinity. Such tunability is based on fluorine's unique physicochemical properties (e.g., low polarizability, relatively small van der Waals radius [1.5 Å, compared to hydrogen (1.2 Å)], and extremely high electronegativity), which may enhance lipophilic interactions and dipolar contacts with the protein target and offer the potential to act as a "true" hydrogen-bond acceptor.[23−26] The replacement of hydrogen with fluorine is the most common structural modification, reflecting the minimal change in steric effect and the increased strength of the C−F bond. On the basis of this premise, the introduction of fluorine to replace hydrogen in the case of **2** might result in enhanced biological activity. While replacement of chlorine with fluorine has less precedent in medicinal chemistry, adopting this approach in the case of anticancer agent **1** offered the intriguing possibility of modulating the proteasome inhibition/recovery profile based on a previously unexploited property of fluorine: its poor leaving group potential. The unique possibilities offered by a fluorinated analogue led to independent reports on the semisynthesis[19] and mutasynthesis[27] of fluorosalinosporamide (**3**). Consistent with the established precedent for enhanced activity for fluorinated compounds compared to their hydrogen-bearing counterparts, **3** was found to be more potent than **2**. In contrast, **3** exhibited decreased potency compared to **1**.[19,27] Most interestingly, the proteasome inhibition/recovery profile of **3** was intermediate between those of **1** and **2**[19,27] and, more generally, between LG and non-LG analogues.[19] On the basis of our proposed mechanism of inhibition/recovery for this class of proteasome inhibitor, we tentatively attributed the unique profile of **3** to slow elimination of fluoride.[19] However, it is difficult to predict the behavior of fluorine substrates (so-called "flustrates").[28] Moreover, fluoride elimination from sp^3 carbons rarely occurs and reportedly only under vigorous conditions (e.g., reflux in the presence of acid or base).[29−31] The notoriously poor LG ability of fluorine[32] suggested that this halogen might remain intact when bound to the proteasome and that its "intermediate" potency and proteasome inhibition/recovery profile might be rooted in other unique properties of fluorine (vide supra), including its potential to act as a hydrogen bond acceptor.[27] Establishing the basis for the unusual behavior of **3** would thus offer critical insights for fine-tuning proteasome inhibition. An intact fluoroethyl group would suggest that this side chain can be modified to exploit interactions within the proteasome S2 binding pocket, which represents a largely open cavity that can be particularly difficult to model. Conversely, fluoride elimination would support the premise that the observed proteasome inhibition/recovery profile is based on LG potential. In this study, we sought to unequivocally elucidate the mechanism for partially reversible proteasome inhibition by **3**. First, we determined the crystal structures of **3** in complex with yeast CP after two distinct incubation times. Then, to explore the potential for hydrogen bonding interactions involving fluorine, we performed a comparative study of the CP in complex with hydroxysalinosporamide (**4**), with the rationale that OH is a superior hydrogen bond acceptor compared to F.[25,26] Furthermore, to investigate whether the LG plays a role in proteasome inhibition post-elimination, the crystal structure of the proteasome CP in complex with bromosalinosporamide (CP/**5**) was determined in an attempt to detect the eliminated bromide ion by taking advantage of anomalous diffraction on the bromine edge. Together, the three selected ligands span the range of irreversible (**5**), partially reversible (**3**), and slow substrate (**4**) inhibitor.[19]

Results

Cocrystallization of Inhibitors with 20S Proteasomes from *S. cerevisiae*. To explore the possibility that slow fluoride elimination renders **3** a partially reversible proteasome inhibitor, crystal structures of CP/**3** complexes were evaluated at two time points. Specifically, **3** was complexed with the yeast 20S proteasome by soaking a single proteasome crystal with **3** for 60 min at a final concentration of 1.25 mM (CP/**3**-1). A second, independent CP/**3** complexation was performed with a long (24 h) soaking time (1.25 mM, CP/**3**-2). The hydroxy group of **4** is not expected to undergo elimination after β-lactone ring-opening;[19] thus, the CP/**4** structure was evaluated after a single long time point (24 h, final concentration of 2.5 mM). In the case of bromosalinosporamide (**5**), rapid halogen elimination is expected;[19] therefore, a single, short crystal soak time (60 min, 2.5 mM) was implemented. To identify whether a released bromide anion is bound at any defined protein receptor position, anomalous data were collected on CP/**5** crystals at the bromine edge.

Crystallographic refinement started from the coordinates of the yeast 20S proteasome[7] followed by anisotropic overall temperature factor correction as well as positional refinement using CNS[33] and cyclic 2-fold symmetry averaging using MAIN.[34] Electron density maps calculated with phases after averaging allowed a detailed interpretation of complexes of the 20S CP with compounds **3**, **4** and **5**. For the scanning of bromine binding sites, an anamolous F_OF_C electron density was calculated. In all cases, the inhibitors occupy all six proteolytic subunits and are covalently bound to the N-terminal threonine residues via the carbonyl carbon atom derived from the β-lactone ring. Since the ligands have previously shown the highest affinity for the CT-like site,[19,21] detailed aspects of each CP/inhibitor complex are discussed with particular focus on the β5 subunit.

Bromosalinosporamide in Complex with the 20S Core Particle (CP/5). Evaluation of the electron density map of CP/**5** (see Supporting Information) indicated that the binding of bromosalinosporamide at the proteasome active sites is analogous to that of **1** (rmsd = 0.02 Å). Specifically, the carbonyl carbon atom derived from the β-lactone ring is covalently bound to the catalytic N-terminal Thr1O$^{\gamma}$, and the C3-O forms a cyclic ether ring with the C-2 side chain as a result of release of bromide, which was entirely complete within the 1 h incubation period in all three subunit types. The bromide anion could not be detected in the anomalous density map, excluding the possibility of a defined anion receptor/binding site at the proteasomal active site concomitant with cyclic ether ring formation. This may suggest total release of the bromide anion from the active site or nondefined binding of the bromide anion. Once released, it appears unlikely that the anion plays a further role in proteasome inhibition subsequent to its critical role in enabling the formation of the irreversibly bound cyclic ether end product (Scheme 1, **Ib**′).

Hydroxysalinosporamide in Complex with the 20S Core Particle (CP/4). In the case of the CP/**4** complex, the experimental electron density map with subunit β5 is shown in Figure 1a. The hydroxyethyl side chain of **4** is pointing into the open S2 binding pocket. This side chain is less well-defined in electron density for subunits β1 and β2, indicating that it is more flexible within these two sites. However, the C-1−C-2−C-12−C-13 dihedral angle is 65 ± 2° across the three subunits, indicating that the side chain adopts a common low energy gauche$^+$ conformation in all three sites (see Supporting Information). In the β5 subunit, there is diffuse electron density associated with a water molecule in proximity to both the side chain hydroxyl group of **4** and Gly23NH (**4**-OH−HOH, 3.0 Å; HOH−Gly23NH, 3.2 Å). Its position suggests the potential to form a bridge between the inhibitor and the proteasome (W6, Figure 1a,b), possibly supporting the relative conformation of the hydroxyethyl side chain compared to the fluoroethyl group of CP/**3**-1 (vide infra). However, the hydroxyethyl side chain is already in a relatively low energy gauche conformation, and the electron density for the water is weak, making its presence and functional significance uncertain.

Fluorosalinosporamide in Complex with the 20S Core Particle (CP/3-1 and CP/3-2). The electron density maps of CP/**3**-1 and CP/**3**-2 (1 and 24 h crystal soak times, respectively) with subunit β5 are captured in Figure 1c,e. The experimental results represent an averaging of electron density and therefore capture the dominant species at each time point; a superposition of the structures is shown in Figure 2. These crystal structures offer striking snapshots of proteasome inhibition by **3** over time and provide new mechanistic insights for the β-lactone−γ-lactam class of inhibitors. The CP/**3**-1 complex depicts an intact fluoroethyl side chain, providing the first view of the halogenated ligand *prior* to LG elimination, while the CP/**3**-2 complex reveals complete elimination of fluoride in all proteolytic subunits, clearly apparent from the cyclic ether end product that is essentially identical to those of CP/**1** and CP/**5**. Superposition of inhibitor molecules from subunits β5 for CP/**1**, CP/**5**, and CP/**3**-2 gave rmsd < 0.05 Å for all atoms (data not shown). Thus, while the average electron density offered no evidence for fluoride elimination after 60 min, the displacement reaction was complete after 24 h. These findings support a two-step reaction with initial, rapid formation of the acyl−enzyme intermediate (CP/**3**-1; formula **Ib**, Scheme 1), followed by slow elimination of fluoride and concomitant formation of the stable cyclic ether end product (CP/**3**-2; formula **Ib**′). In CP/**3**-1, the conformation of the fluoroethyl side chain (−44° in β5; −42 ± 8° across three subunits for dihedral angle C-1−C-2−C-12−C-13; see Supporting Information) is distinct from that observed for CP/**4** (+65°, vide supra) (Figure 2) and might be stabilized by favorable hydrophobic van der Waals interactions with the aromatic side chain of Tyr168 (F−Tyr168, 3.7 Å; F−Tyr168, 3.8 Å, for two carbon atoms of the aromatic ring) in subunit β5. The overall architecture of the ligand within the binding site seems to anticipate fluoride elimination. The well-defined fluoroethyl side chain requires a relatively modest change in the C-1−C-2−C-12−C-13 dihedral angle (−40° rotation) to achieve the final conformation of the five-membered cyclic ether found in CP/**3**-2 (−84°), and the terminal carbon (C-13) bearing fluorine is in proximity to C-3O, which will ultimately displace it. Remarkably, C-13 (CH$_2$F) is 3.1 Å from C-3O, approximating the sum of their van der Waals radii and strongly indicating that the fluoroethyl side chain has adopted a nearly optimal conformation for fluoride elimination. Moreover, C-3O is 2.8 Å from the free N-terminus (Thr1NH$_2$), strongly supporting the role of the free amino group as the catalyst for the intramolecular nucleophilic displacement reaction. Interestingly, the fluorine atom in the β5 subunit of the CP/**3**-1 structure is surrounded by a remarkably well-defined network of water molecules (W1−W5, Figure 1d) that were not detected in CP/**3**-2 (i.e., after fluoride elimination) or in any yeast proteasome crystal structure to date. The most proximal water molecule, W2, is juxtaposed between F (F−O, 2.6 Å) and W1 (O−O, 2.6 Å), indicating that W2 forms a hydrogen bond bridging F and W1.[25,26] On the basis of its relative position (S129NH, 3.1 Å; S129OH, 3.1 Å; C-3O, 2.8 Å), W1 may represent the dominant nucleophile of the water molecule cluster involved in substrate hydrolysis[22,35] that has been displaced by C-3O upon ligand binding. The fluorine atom is also proximal to three other well-defined water molecules, W3, W4, and W5. The excellent electron density and the nature in which these five water molecules surround the fluorine atom may suggest structural and/or mechanistic relevance, such as solvation of the anion upon its release. Overall, the CP/**3**-1 structure embodies numerous features consistent with a ligand in anticipation of leaving group elimination, including a side chain conformation that renders the ligand (C-3O and C-13) and the active site catalytic N-terminus suitably organized for nucleophilic displacement of fluorine, with the potential for fluoride anion solvation by proximal water molecules

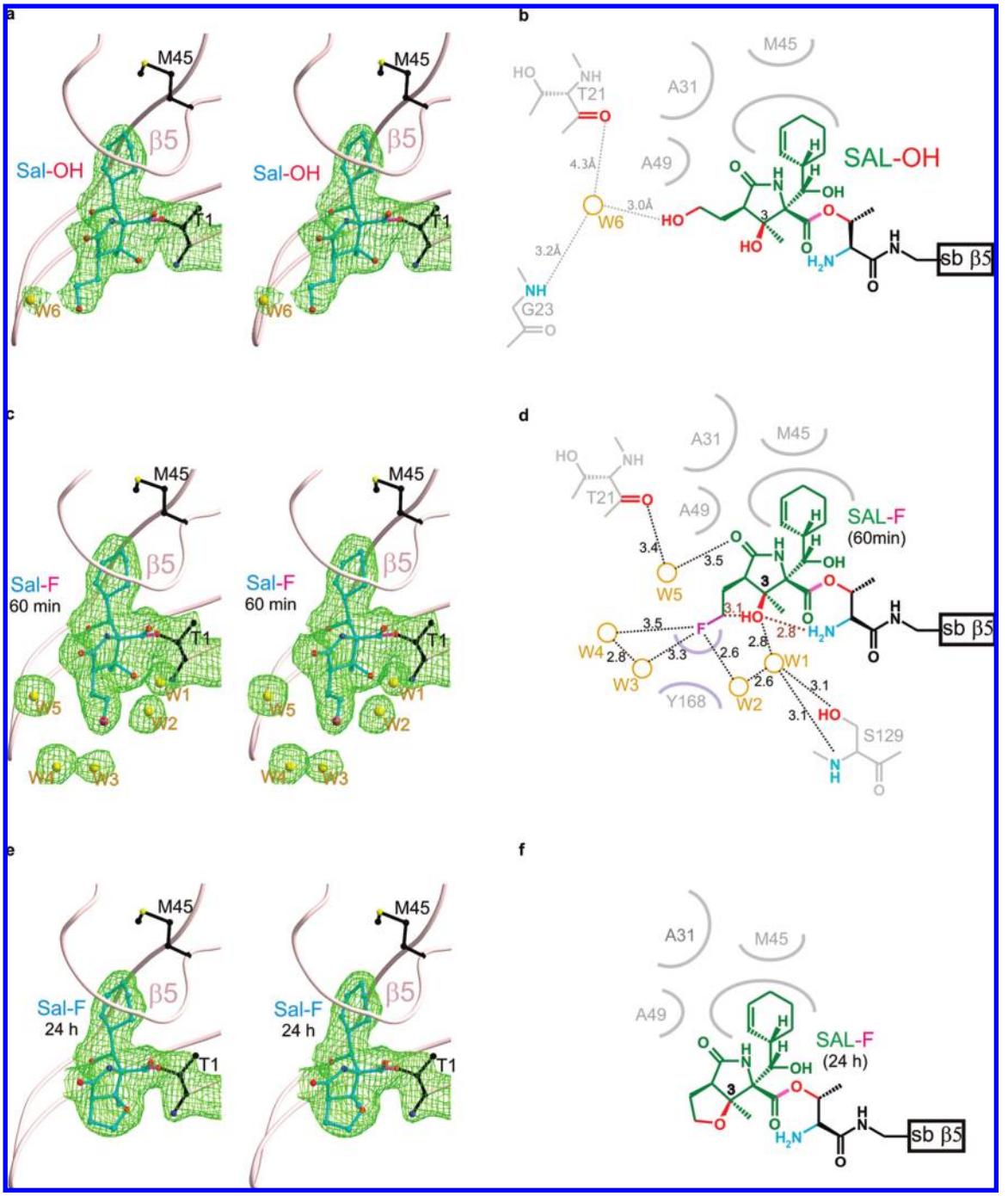

Figure 1. Electron density and two-dimensional contact maps for compounds **3** and **4** in complex with the 20S CT-L site. Stereorepresentation of the CT-L active site of the yeast 20S proteasome in complex with **4** (Sal−OH) (a), **3**-1 (Sal-F, 60 min) (c), and **3**-2 (Sal-F, 24 h) (e). Covalent linkage of the inhibitor with β5-Thr1O$^{\gamma}$ is drawn in magenta. The electron density map (colored in green) is contoured from 1σ around Thr1 (colored in black) with $2F_O - F_C$ coefficients after 2-fold averaging. Temperature factor refinement indicates full occupancies of the inhibitor binding site. The ligands have been omitted for phasing. Schematic overview of **4** (b), **3**-1 (d), and **3**-2 (f) and amino acids of the ligand binding site of the 20S proteasome. Hydrogen bonds with their correlated distances between heavy atoms in Å are shown as black broken lines, whereas the characteristic oxygen and nitrogen atoms are presented in red and blue capitals, respectively. Nonpolar hydrogen interactions are drawn as gray cycle segments. Water molecules are shown as yellow spheres. The distances between atoms involved in nucleophilic displacement of fluoride (Thr1N, C3-O, and C-13) are highlighted as brown broken lines (d).

after elimination, together giving rise to the highly stabilized cyclic ether end product observed in CP/**3**-2. The species involved in this two-step proteasome inhibition reaction sequence, trapped in crystal structures of the 20S CP in complex with **3** by virtue of slow fluoride elimination, may be viewed as "freeze-frame" windows into the analogous mechanism for anticancer agent **1**.

pH Dependence of Halide Elimination in Aqueous Buffer. The ability of the proteasome active site to catalyze the uncommon reaction of fluoride displacement from an sp^3 carbon demonstrates the effectiveness of the free base (Thr1NH$_2$). The analogous intramolecular fluoride elimination reaction for **3** (**Ia** → **Ia**′, Scheme 1) is exceedingly slow in aqueous buffer (≥5 days at pH 7.3, 37 °C),[19] and independent

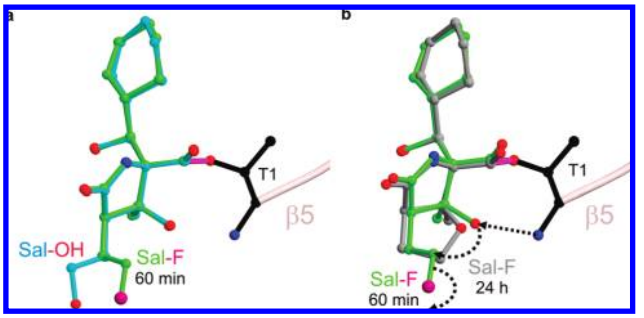

Figure 2. Structural superimpositions at the CT-L site: (a) **3**-1 (Sal-F, 60 min, colored in green) and **4** (Sal−OH, cyan); (b) **3**-1 (Sal-F, 60 min, green) and **3**-2 (Sal-F, 24 h, gray), including Thr1 (black) and covalent linkage of the inhibitor with β5-Thr1O$^{\gamma}$ (magenta). The structural superimpositions clearly indicate structural rearrangements of side chains in salinosporamides in a unique way before and after completion of the five-membered ether ring formation, thereby changing the inhibitor binding mode on the proteasome from reversible to irreversible.

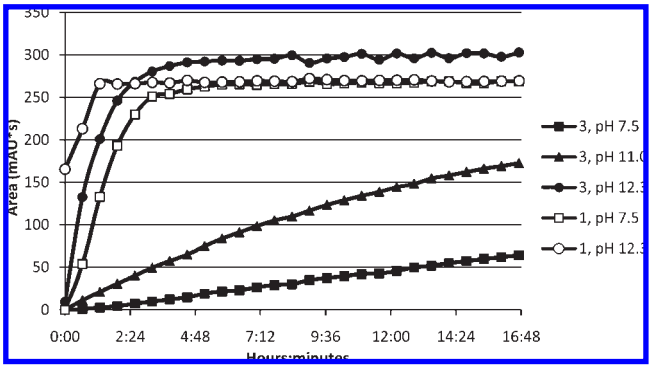

Figure 3. pH dependence of halide elimination from **1** and **3** in aqueous buffer.

reports of intramolecular displacement of fluoride to form cyclic ethers required vigorous conditions.[29−31] The kinetics of the more facile chloride elimination from **1** in aqueous buffer have been reported previously; the reaction rate was pH-independent from pH 4.5 to pH 6.5 and increased at pH > 7.[36] While the pK_a of C-3OH is not known, it is reasonable to expect it to be similar to that of other tertiary alcohols (> 14). Thus, chloride displacement at low to neutral pH suggests that C-3OH, in the form of the alcohol, can act as the nucleophile.[37] The nucleophilicity of C-3O should increase with pH to enhance the rate of halide displacement, consistent with the reported rate increase from pH 7 to pH 8 or 9.[36] To extend our understanding of the pH-dependence of halide elimination from **1** and **3** to the high pH range, β-lactone ring-opening and subsequent halide displacement were monitored by HPLC at 37 °C in phosphate buffer (25 mM) from pH 7.5 to pH 12.3. Hydrolysis of the β-lactone was previously established to occur at the same rate for **1** and **3** and to precede halide displacement,[19] allowing us to focus on the latter step (**Ia** → **Ia**′, Scheme 1). The results clearly demonstrated that fluoride elimination occurred more rapidly with increasing pH (Figure 3). The time course for fluoride elimination at pH 12.3 (which begins to approach the pK_a of an alcohol) approximated that of chloride elimination at pH 7.5, which may reflect the increased nucleophilicity/higher concentration of C3-O$^-$ (anionic state) required to drive the S_N2 reaction in the case the stronger carbon−fluorine bond.

Discussion

Anticancer agent **1** exhibits prolonged duration proteasome inhibition in vitro and in vivo;[13,19] moreover, packed whole blood lysates obtained from patients in phase I clinical trials show sustained inhibition of all three 20S proteolytic activities after intravenous administration of **1**.[20] The crystal structure of **1** in complex with the 20S proteasome provided a strong case for the role of the LG in the mechanism for irreversible binding,[22] and inhibition/recovery studies of analogues bearing LG substituents in place of chlorine demonstrated that a good LG imparts prolonged duration proteasome inhibition (no recovery of activity after 24 h of dialysis) compared to non-LG analogues (full recovery of activity, ≤12 h).[19] A mechanism was proposed (Scheme 1) whereby non-LG analogues act as slow substrates that are ultimately removed from the proteolytic active site by either re-formation of the β-lactone ring (pathway C) or aqueous hydrolysis (pathway D), with steric interference by C-3O attenuating the latter pathway.[19,22] These two possible competing pathways for cleaving the inhibitor−proteasome ester linkage are putatively catalyzed by the free N-terminus (Thr1NH$_2$). In the case of **1** and LG analogues, LG elimination (pathway E) presents a competing pathway that apparently occurs much more rapidly than pathway C and/or pathway D. Moreover, once the LG has been eliminated, there is no effective means of hydrolyzing the ester linkage between the inhibitor and Thr1O$^{\gamma}$; the β-lactone ring cannot re-form, as C-3O is confined within the cyclic ether ring, and aqueous hydrolysis is limited by steric interference by C-3O, together with a catalytically inactivated (protonated, at least temporally) N-terminus (Thr1NH$_3^+$).[22] Thus, **1** and LG analogues (in the form of **Ib**′) are rendered irreversibly bound.[19,22] Interestingly, fluorosalinosporamide (**3**) exhibited an intermediate proteasome inhibition/recovery profile compared to LG and non-LG analogues, with only partial recovery of CT-L activity after dialysis.[19] Insights obtained from crystal structures of **3** in complex with the 20S CP demonstrate that the mechanism for partially reversible proteasome inhibition is indeed based on slow elimination of fluoride catalyzed by the free N-terminus (Scheme 1). After formation of the acyl−enzyme adduct, intermediate **Ib** (observed in crystal structure CP/**3**-1), the rate of LG elimination is sufficiently attenuated (because of the poor LG properties of fluorine) such that pathways C (β-lactone reformation) and D (aqueous hydrolysis) become competitive with pathway E (LG elimination). As a result, a fraction of bound inhibitor **3** may be removed from the active site (via pathway C and/or pathway D), while another fraction may be converted to the irreversibly bound cyclic ether end product **Ib**′ via pathway E, as found in crystal structure CP/**3**-2. Such competition results in partial recovery of proteolytic activity (resulting from the hydrolyzed fraction) and ultimately stabilization to a constant level of inhibition (attributed to the irreversibly bound fraction).[19] Kinetically, **3** behaves as a slow substrate (in the form of (CB/**3**-1; **Ib**) that undergoes in situ transformation to an irreversible inhibitor (CP/**3**-2; **Ib**′). In summary, attenuating the LG potential of the ligand by replacement of chlorine (**1**) with fluorine (**3**) modulates the proteasome inhibition profile from that of a true irreversible inhibitor to a partially reversible inhibitor.

The ligand's behavior as a slow substrate versus irreversible inhibitor will affect the extent and duration of proteasome inhibition, thereby contributing to potency. Previously established IC$_{50}$ values for inhibition of the CT-L activity of

isolated 20S proteasomes (IC_{50}(**5**) = 2.6 nM < IC_{50}(**3**) = 9.2 nM < IC_{50}(**4**) = 14 nM) are inversely correlated with LG potential (Br > F > OH), partially reflecting contributions from irreversible binding but also the enthalpies and entropies associated with LG elimination.[19,21] For a covalent adduct, ligand binding affinity, reaction energetics at the binding site, and the off rate (k_{off}) from the target must all be considered. For example, while **1**, **3**, **4**, and **5** all have substituted ethyl side chains that adopt more defined conformations upon ligand binding and recognition by the active site (followed by cyclic ether formation in the cases of **1**, **3**, and **5**), this decrease in entropy can be offset by anion elimination (entropy increase) when the ligand bears a LG. Inability to detect the bromide anion in the anomalous density map indicated that there is no defined LG anion receptor binding site at the proteasomal active site, consistent with an entropy increase. Contributions from reaction enthalpies include relative LG potential, i.e., the less facile elimination of fluoride compared to superior LGs (e.g., chloride and bromide of **1** and **5**, respectively). Finally, in terms of k_{off} rates, non-LG analogue **4** behaves as a slow substrate that is slowly eliminated from the binding pocket, **1** and **5** are irreversibly bound, and **3** behaves intermediately.[19] Indeed, many of the contributions to binding energetics and potency outlined above relate to the absence or presence and nature of the LG, including irreversible binding, which will enhance the extent of proteasome inhibition. However, the IC_{50} values for inhibition of CT-L activity of isolated proteasomes are all in the low nanomolar range,[19] and the most significant consequences of irreversible binding may be on downstream cellular events and efficacy (vide infra).

Proteasome-catalyzed fluoride elimination begs the question of the Thr1N pK_a. In contrast to the serine proteases, for which the catalytic His57 pK_a has been the subject of in-depth studies, the 20S proteasome Thr1N pK_a has not been reported. By use of serine proteases as a parallel case of an enzyme catalyzing peptide bond hydrolysis, the optimal His57 pK_a was expected to fall between 9 and 14, i.e., sufficiently high to abstract a proton from the nucleophile (Ser195OH; p$K_a \approx 14$) but not so high as to prohibit proton transfer to the amine leaving group of the cleaved peptide.[38] Detailed studies by Frey and co-workers demonstrated that the His57 pK_a is effectively raised upon ligand binding via a conformational change, with concomitant formation of a low barrier hydrogen bond with the proximal Asp102 carboxylate side chain in this classic case.[38−40] Using trifluoroketone inhibitors in complex with chymotrypsin, observed His57 pK_a values (∼10−12) were established to fall within the expected optimal range. In the proteasome, the analogous peptide bond cleavage reaction is catalyzed within a unique active site architecture in which Thr1N (in concert with a water molecule acting as proton shuttle) assumes a similar role to His57, while Thr1OH acts as the nucleophile. By analogy, it is plausible that the Thr1 pK_a may be in a similar range to that of His57 in the ligated form, enhancing its ability to catalyze proton abstraction from the Thr1OH alcohol. In the presence of inhibitors **1** and **3**, an elevated Thr1N pK_a could also increase the nucleophilicity of tertiary alcohol C-3OH and accelerate S_N2 displacement of the halide. In general, the free N-terminal α-amino group of a protein has an "expected" pK_a of ∼6.8−7.9.[41] If the proteasome free N-terminus (Thr1N) pK_a is inherently high (e.g., 10−12) prior to ligand binding, it should be fully protonated at physiological pH and therefore unavailable for catalysis. Thus, a *catalytic* N-terminus may require pK_a elevation upon ligand binding to "activate" proton abstraction from Thr1OH, akin to that of serine proteases. Conversely, the Thr1OH could be induced to become more acidic (pK_a reduction). While a network of neighboring residues with potential to interact with and modulate the pK_a of Thr1N and Thr1OH has been described,[7] the value of the Thr1N pK_a and whether it might be raised upon ligand binding and/or over the course of substrate hydrolysis remain to be established.

What can halide elimination from **1** and **3** tell us about proteasome substrate hydrolysis and active site pK_a values? Upon reaction with β-lactone inhibitors, the enzyme−inhibitor complex is structurally analogous to the acyl−enzyme adduct during peptide substrate hydrolysis.[6,7] In this case, the inhibitor C-3OH occupies the position of the nucleophilic water that would generally cleave the acyl−enzyme bond.[22] Thus, monitoring proton transfer in β-lactone adducts, including proton abstraction from C-3OH, may provide insights into the more broadly applicable deacylation reaction. While model experiments in aqueous solution cannot mimic enhanced catalysis in the active site that may occur through proximity and orientation (e.g., Thr1N to C-3O, which are within hydrogen bonding distance in the proteasome active site), other energetically favorable aspects unique to an enzyme active site, such as potential contributions from induced fit, may be less relevant in this case given that halide elimination occurs within the open S2 cavity; furthermore, the geometry of C-12−C-2−C-3−C-3O is fixed and essentially identical in both the proteasome active site and aqueous solution. Moreover, C-3OH only makes contact with Thr1N, strongly reducing the possibility that the C-3OH pK_a is being influenced by other neighboring residues and further suggesting that C-3OH behaves like a typical tertiary alcohol. Thus, optimal pH values for halide elimination reactions in aqueous solution may provide some predictive value with respect to the Thr1N pK_a. In the case of **1**, nucleophilic displacement of chloride by C-3O occurred in aqueous buffer at physiological pH, while fluoride elimination from **3** was exceedingly slow (Figure 3). At pH 11, fluoride elimination was still only ∼50% complete after ∼12 h. At pH 12.3, fluoride elimination was markedly accelerated; the reaction was complete within ∼5 h, while chloride elimination was complete after ≤1.3 h. These latter time frames approximate those estimated from independent studies demonstrating partial or complete recovery of proteasome inhibition by **3** or **1**, respectively, after room temperature dialysis.[19] Moreover, Moore and co-workers previously demonstrated irreversible binding by **1** after only 15 min of preincubation at 37 °C,[27] further supporting rapid chloride elimination in the proteasome active site. Accelerated halide elimination with increasing aqueous buffer pH, together with currently available data on the time frames for irreversible binding to the proteasome, is suggestive of a proteasome active site Thr1N pK_a > 10, which is consistent with the analogy drawn from serine proteases (vide supra). While this rationale requires many assumptions, it suggests that a detailed kinetic evaluation of proteasome inhibition/recovery by **1** and **3** over a range of pH values, in concert with crystallographic analysis, may offer a viable strategy to formally establish the proteasome Thr1N pK_a.

Concluding Remarks

The importance of a LG to the proteasome inhibition profile of **1** and analogues is now well established.[19,22] The fluorosalinosporamide/CP structure CP/**3**-1 presented herein

provides the first view of the ligand *prior* to LG elimination, captured by virtue of the poor LG ability of fluoride. A snapshot in subunit β5 at the 1 h crystal soak time reveals the inhibitor prearranged for fluoride elimination, with (i) a well-defined fluoroethyl side chain conformation, (ii) $\underline{C}H_2F$ within van der Waals distance of the C-3$\underline{O}$ nucleophile that will displace fluoride, (iii) Thr1$\underline{N}$ within hydrogen bonding distance of C-3$\underline{O}$, supporting its role as a catalyst for the intramolecular nucleophilic displacement reaction, and (iv) fluorine proximal to a network of well-defined, low entropy water molecules that may solvate the anion upon its release. Fluoride elimination was complete after 24 h of crystal soak time, giving cyclic ether end product (CP/**3**-2). These findings provide a rare example of fluoride displacement from an sp^3 carbon in the context of an enzyme active site and offer preliminary insights into the active site Thr1N pK_a. The ability to trap the ligand before and after fluoride elimination is consistent with the behavior of fluorosalinosporamide as a partially reversible proteasome inhibitor and gives credence to the general mechanism outlined in Scheme 1 for this class of inhibitor, opening the door for further exploitation of this pathway for fine-tuning proteasome inhibition. Effective modulation of the proteasome inhibition profile by introduction of fluorine provides yet another compelling example of the utility of fluorine in medicinal chemistry but uniquely based on its property as a LG.

Modulating the equilibrium of proteasomal protein degradation may cause irreversible effects on cell behavior. Previous studies indicated that LG analogues are ~3 log units more cytotoxic to RPMI 8226 cells compared to non-LG analogues.[21] Cell response to the ligand depends on a variety of properties, including its half-life, metabolism profile, affinity constant, and k_{off} rate from its molecular target. As it is now possible to design analogues with profiles that span the LG (true "irreversible inhibitors") and non-LG ("slow substrate") analogues, as exemplified by fluorosalinosporamide, the impact of k_{off} on cellular events downstream of the proteasome can be probed directly. Recent studies in leukemia cells indicate that LG analogues enhance induction of reactive oxygen species for prolonged periods compared to non-LG analogues and more effectively activate caspase-8. Both processes occur downstream of proteasome inhibition.[42] Fine tuning the duration of proteasome inhibition may have important therapeutic implications for the treatment of cancer, inflammation, and infectious diseases.

Experimental Section

Synthetic Protocols. Compounds **3** and **4** were prepared by semisynthesis, identified by spectroscopic methods, and evaluated for purity by analytical HPLC (98.4% and 98.8%, respectively), all as described previously.[19] Compound **5** was prepared by fermentation of *Salinispora tropica* using a stepwise NaBr-enrichment scheme followed by repetitive chromatography of the crude extract as described previously.[43] The identity of **5** was confirmed by spectroscopic methods and purity was determined by analytical HPLC (95.8%), also described previously.[43]

pH Dependence of Halide Elimination from Compounds 1 and 3. β-Lactone hydrolysis and halide elimination from **1** and **3** were monitored by HPLC over time in phosphate buffer (25 mM Na_2HPO_4) at 37 °C. The pH of the buffer solution was adjusted to 7.5, 11.0, or 12.3 with either 0.1 M NaOH or 0.1 M HCl using a Beckman pH meter. The buffer solution was pre-equilibrated at 37 °C for 30 min on an HPLC autosampler (Agilent 1200). Compounds were prepared as 1 mg/mL stock solutions in acetonitrile, and aliquots (20 μL) were spiked into pre-equilibrated buffer (980 μL) to a final concentration of 20 μg/mL. The solutions were analyzed over time by sequential injection of 25 μL aliquots onto an Agilent analytical HPLC 1200 system equipped with a photodiode array detector and a C-18 column (ACE 3 C18, 150 mm × 4.6 mm, column temperature of 30 °C). The HPLC mobile phases were A (0.01% aqueous TFA) and B (0.01% TFA in acetonitrile). The gradient commenced with 100% A (1 min) followed by linear increase to 100% B over the next 15 min at a flow rate of 1 mL/min. HPLC autosampler temperature (37°C) was monitored periodically with an external temperature probe. The starting materials and halide elimination products were identified by their established HPLC retention times. The UV area (mAU·s) for **Ia**′ was plotted against HPLC injection time using Microsoft Office Excel 2007.

Cocrystallization. Crystals of the 20S proteasome from *S. cerevisiae* were grown in 2 μL hanging drops at 24 °C under 0.1 M morpholinoethanesulfonic acid (MES) (pH 6.8), 25 mM $MgAc_2$, and 9% 2-methyl-2,4-pentanediol (MPD) buffer conditions as previously described.[44] Growth of crystals was completed within 72 h; these crystals were then incubated for 60 min with either 0.5 μL of fluorosalinosporamide (**3**) or 0.5 μL of bromosalinosporamide (**5**). Soaked crystals were transferred to a 5 μL drop of cryoprotectant [0.025 M Tris (pH 7.5), 25 mM $MgAc_2$, and 30% MPD] for 5 min and subsequently were amorphously cooled to 100 K by steam freezing using liquid nitrogen. Crystal mounting and data collection were performed at the synchrotron at the Swiss Light Source, Paul-Scherrer-Institute, Villingen, Switzerland. Long time soaks were performed by adding 5 μL of cryoprotectant [0.025 M Tris (pH 7.5), 25 mM $MgAc_2$, and 30% MPD] to the crystallization drop followed by 0.5 μL of either hydroxysalinosporamide (**4**) or 0.5 μL of fluorosalinosporamide (**3**) for 24 h. Crystals were directly mounted out of the drop, and data collection was performed as described above for the short time soaks of **3** and **5**.

The space group belongs to $P2_1$ with cell dimensions of about a = 135 Å, b = 301 Å, c = 144 Å, and β = 113° (see Supporting Information). Data to 2.5 Å were collected using synchrotron radiation with λ = 1.0 Å and λ = 0.9196 Å in the case of **5** at the bromine absorption edge at the X06SA-beamline in SLS, Villingen, Switzerland. Crystals were soaked in a cryoprotecting buffer (30% MPD, 20 mM magnesium acetate, 100 mM morpholinoethanesulfonic acid, pH 6.9) and frozen in a stream of liquid nitrogen gas at 90 K (Oxford Cryo Systems). X-ray intensities and data reduction were evaluated by using the XDS program package.[45] The anisotropy of diffraction was corrected by an overall anisotropic temperature factor by comparing observed and calculated structure amplitudes using the program CNS.[33] Electron density was improved by averaging and back-transforming the reflections 10 times over the 2-fold noncrystallographic symmetry axis using the program package MAIN.[34] Conventional crystallographic rigid body, positional, and temperature factor refinements were carried out with CNS using the yeast 20S proteasome structure as starting model.[7] Modeling experiments were performed using the coordinates of yeast 20S proteasome with the program MAIN.

The atomic coordinates for the hydroxysalinosporamide/proteasome CP and fluorosalinosporamide/proteasome CP complexes have been deposited with the Protein Data Bank, Research Collaboratory for Structural Bioinformatics at Rutgers University (CP/**3**-1, PDB code 3GPT; CP/**3**-2, PDB code 3GPW; CP/**4**, PDB code 3HYE).

Acknowledgment. We thank R. Feicht for large scale purification of yeast 20S proteasomes and A. Konig, who crystallized the yeast 20S proteasome in complex with the ligands. We also thank S. Neuteboom and J. Weiss for collaborative biology leading up to these studies.

Supporting Information Available: Electron density and two-dimensional contact maps for bromosalinosporamide (**5**) in complex with the 20S CT-L site; structural superimpositions of ligands **3** and **4** at the CT-L (β5), T-L (β2), and C-L (β1) sites; supplementary data collection and refinement statistics. This material is available free of charge via the Internet at http://pubs.acs.org.

References

(1) Adams, J. *Proteasome Inhibitors in Cancer Therapy*; Humana Press: Totowa, NJ, 2004.

(2) Orlowski, R. Z.; Kuhn, D. J. Proteasome Inhibitors in Cancer Therapy: Lessons from the First Decade. *Clin. Cancer Res.* **2008**, *14*, 1649–1657.

(3) Bross, P. F.; Kane, R.; Farrell, A. T.; Abraham, S.; Benson, K.; Brower, M. E.; Bradley, S.; Gobburu, J. V.; Goheer, A.; Lee, S.-L.; Leighton, J.; Liang, C. Y.; Lostritto, R. T.; McGuinn, W. D.; Morse, D. E.; Rahman, A.; Rosario, L. A.; Verbois, S. L.; Williams, G.; Wang, Y.-C.; Pazdur, R. Approval Summary for Bortezomib for Injection in the Treatment of Multiple Myeloma. *Clin. Cancer Res.* **2004**, *10*, 3954–3964.

(4) Richarson, P. G.; Barlogie, B.; Berenson, J.; Singhal, S.; Jagannath, S.; Irwin, D.; Rajkumar, S. V.; Srkalovic, G.; Alsina, M.; Alexanian, R.; Seigel, D.; Orlowski, R. Z.; Kuter, D.; Limentani, S. A.; Lee, S.; Hideshima, T.; Esseltine, D. L.; Kauffman, M.; Adams, J.; Schenkein, D. P.; Anderson, K. C. A Phase 2 Study of Bortezomib in Relapsed, Refractory Myeloma. *N. Engl. J. Med.* **2003**, *348*, 2609–2617.

(5) Groll, M.; Bochtler, M.; Brandstetter, H.; Clausen, T.; Huber, R. Molecular Machines for Protein Degradation. *ChemBioChem* **2005**, *6*, 222–256.

(6) Lowe, J.; Stock, D.; Jap, B.; Zwickl, P.; Baumeister, W.; Huber, R. Crystal Structure of the 20S Proteasome from the Archaeon *T. acidophilum* at 2.4 Å Resolution. *Science* **1995**, *268*, 533–539.

(7) Groll, M.; Ditzel, L.; Lowe, J.; Stock, D.; Bochtler, M.; Bartunik, H. D.; Huber, R. Structure of 20S Proteasome from Yeast at 2.4 Å Resolution. *Nature* **1997**, *386*, 463–471.

(8) Groll, M.; Huber, R. Inhibitors of the Eukaryotic 20S Proteasome Core Particle: A Structural Approach. *Biochim. Biophys. Acta* **2004**, *1695*, 33–44.

(9) Moore, B. S.; Eustaquio, A. S.; McGlinchey, R. P. Advances in and Applications of Proteasome Inhibitors. *Curr. Opin. Chem. Biol.* **2008**, *12*, 434–440.

(10) Borissenko, L.; Groll, M. 20S Proteasome and Its Inhibitors: Crystallographic Knowledge for Drug Development. *Chem. Rev.* **2007**, *107*, 687–717.

(11) Feling, R. H.; Buchanan, G. O.; Mincer, T. J.; Kauffman, C. A.; Jensen, P. R.; Fenical, W. Salinosporamide A: A Highly Cytotoxic Proteasome Inhibitor from a Novel Microbial Source, a Marine Bacterium of the New Genus *Salinospora*. *Angew. Chem., Int. Ed.* **2003**, *42*, 355–357.

(12) Fenical, W.; Jensen, P. R.; Palladino, M. A.; Lam, K. S.; Lloyd, G. K.; Potts, B. C. Discovery and Development of the Anticancer Agent Salinosporamide A (NPI-0052). *Bioorg. Med. Chem.* **2009**, *17*, 2175–80.

(13) Chauhan, D.; Catley, L.; Li, G.; Podar, K.; Hideshima, T.; Velankar, M.; Mitsiades, C.; Mitsiades, N; Yasui, H.; Letai, A.; Ovaa, H.; Berkers, C.; Nicholson, B.; Chao, T.-H.; Neuteboom, S. T. C.; Richardson, P.; Palladino, M. A.; Anderson, K. C. A Novel Orally Active Proteasome Inhibitor Induces Apoptosis in Multiple Myeloma Cells with Mechanisms Distinct from Bortezomib. *Cancer Cell* **2005**, *8*, 407–419.

(14) Chauhan, D.; Hideshima, T.; Anderson, K. C. A Novel Proteasome Inhibitor NPI-0052 as an Anticancer Therapy. *Br. J. Cancer* **2006**, *95*, 961–965.

(15) Cusack, J.; Liu, R.; Xia, L.; Pien, C.; Niu, W.; Palombella, V.; Chao, T-H.; Neuteboom, S. T. C.; Palladino, M. A. NPI-0052 Enhances Tumoricidal Response to Conventional Cancer Therapy in a Colon Cancer Model. *Clin. Cancer Res.* **2006**, *12*, 6758–6764.

(16) Sloss, C. M.; Wang, F.; Liu, R.; Houston, M.; Ljungman, D.; Palladino, M. A.; Cusack, J. C. Proteasome Inhibition Activates Epidermal Growth Factor Receptor (EGFR) and EGFR-Independent Mitogenic Kinase Signaling Pathways in Pancreatic Cancer Cells. *Clin. Cancer Res.* **2008**, *14*, 5116–5123.

(17) Aghajanian, C. A.; Hamlin, P.; Gordon, M. S.; Hong, D. S.; Naing, A.; Younes, A.; Hannah, A.; Palladino, M. A.; Spear, M. A.; Kurzrock, R. Phase I Study of the Novel Proteasome Inhibitor NPI-0052 in Patients with Lymphoma and Solid Tumors. *J. Clin. Oncol., Suppl.* **2008**, *26* (15S, Part 1 of 2), 171S; Abstract 3574.

(18) Padrik, P.; Price, T. J.; Spear, M. A.; Townsend, A.; Longenecker, A.; Palladino, M. A.; Lloyd, G. K.; Cropp, G. F.; Millward, M. Phase I Study of the Novel Proteasome Inhibitor NPI-0052 in Patients with Advanced Malignancies Including Leukemias. *Ann. Oncol.* **2008**, *19* (Suppl. 8), viii162, 489P.

(19) Manam, R. R.; M^{c}Arthur, K. A.; Chao, T.-H.; Weiss, J.; Ali, J. A.; Palombella, V. J.; Groll, M.; Lloyd, G. K.; Palladino, M. A.; Neuteboom, S. T. C.; Macherla, V. R.; Potts, B. C. M. Leaving Groups Prolong the Duration of 20S Proteasome Inhibition and Enhance the Potency of Salinosporamides. *J. Med. Chem.* **2008**, *51*, 6711–6724.

(20) Palladino, M. A.; Chao, T-H.; Neuteboom, S. T. C.; Spear, M.; Ma, W.; Albitar, M. Preclinical and Clinical Monitoring of Cell and Circulating Plasma Specific Proteasome Biomarkers after Treatment with the Proteasome Inhibitor NPI-0052. *EJC Suppl.* **2008**, *6* (12), 74; Abstract 235 .

(21) Macherla, V. R.; Mitchell, S. S.; Manam, R. R.; Reed, K.; Chao, T.-H.; Nicholson, B.; Deyanat-Yazdi, G.; Mai, B.; Jensen, P. R.; Fenical, W.; Neuteboom, S. T. C.; Lam, K. S.; Palladino, M. A.; Potts, B. C. M. Structure−Activity Relationship Studies of Salinosporamide A (NPI-0052), a Novel Marine Derived Proteasome Inhibitor. *J. Med. Chem.* **2005**, *48*, 3684–3687.

(22) Groll, M.; Huber, R.; Potts, B. C. M. Crystal Structures of Salinosporamide A (NPI-0052) and B (NPI-0047) in Complex with the 20S Proteasome Reveal Important Consequences of β-Lactone Ring Opening and a Mechanism for Irreversible Binding. *J. Am. Chem. Soc.* **2006**, *128*, 5136–5141.

(23) Bohm, H.-J.; Banner, D.; Bendels, S.; Kansy, M.; Kuhn, B.; Muller, K.; Obst-Sander, U.; Stahl, M. Fluorine in Medicinal Chemistry. *ChemBioChem* **2004**, *5*, 637–643.

(24) Biffinger, J. C.; Kim, H. W.; DiMagno, S. G. The Polar Hydrophobicity of Fluorinated Compounds. *ChemBioChem* **2004**, *5*, 622–627.

(25) Howard, J. A. K.; Hoy, V. J.; O'Hagen, D.; Smith, G. T. How Good Is Fluorine as a Hydrogen Bond Acceptor? *Tetrahedron* **1996**, *38*, 12613–12622.

(26) Dunitz, J. D.; Taylor, R. Organic Fluorine Hardly Ever Accepts Hydrogen Bonds. *Chem. Eur. J.* **1997**, *3*, 89–98.

(27) Eustaquio, A. S.; Moore, B. S. Mutasynthesis of Fluorosalinosporamide, a Potent and Reversible Inhibitor of the Proteasome. *Angew. Chem., Int. Ed.* **2008**, *47*, 3936–3938.

(28) Seebach, D. Organic Synthesis. Where Now? *Angew. Chem., Int. Ed.* **1990**, *29*, 1320–1367.

(29) Saulnier, M. G.; Langley, D. R.; Frennesson, D. B.; Long, B. H.; Huang, S.; Gao, Q.; Wu, D.; Fairchild, C. R.; Ruediger, E.; Zimmermann, K.; St. Laurent, D. R.; Balasubramaniam, B. N.; Vyas, D. M. Novel 3′,6′-Anhydro and N12,N13-Bridged Glycosylated Fluoroindolo[2,3-*a*]carbazoles as Topoisomerase I Inhibitors. Fluorine as a Leaving Group from sp^3 Carbon. *Org. Lett.* **2005**, *7*, 1271–1274.

(30) Djuric, S. W.; Garland, R. B.; Nysted, L. N.; Pappo, R.; Plume, G.; Swenton, L. Synthesis of 5-Fluoroprostacyclin. *J. Org. Chem.* **1987**, *52*, 978–990.

(31) Toscano, L.; Fioriello, G.; Silingardi, S.; Inglesi, M. Preparation of (8*S*)-8-Fluoroerythronolide A and (8*S*)-8-Fluoroerythronolide B, Potential Substrates for the Biological Synthesis of New Macrolide Antibiotics. *Tetrahedron* **1984**, *40*, 2177–2181.

(32) Jaramillo, P.; Domingo, L. R.; Perez, P. Towards an Intrinsic Nucleofugality Scale: The Leaving Group (LG) Ability in CH_3LG Model System. *Chem. Phys. Lett.* **2006**, *420*, 95–99.

(33) Brünger, A.; Adams, P.; Clore, G.; DeLano, W.; Gros, P.; Grosse-Kunstleve, R.; Jiang, J.; Kuszewski, J.; Nilges, M.; Pannu, N.; Read, R.; Rice, L.; Simonson, T.; Warren, G. Crystallography & NMR System: A New Software Suite for Macromolecular Structure Determination. *Acta Crystallogr., Sect. D.* **1998**, *1*, 905–921.

(34) Turk, D. Improvement of a Program for Molecular Graphics and Manipulation of Electron Densities and Its Application for Protein Structure Determination. Thesis, Technische Universität München, Germany, 1992.

(35) Groll, M.; Balskus, E. P.; Jacobsen, E. N. Structural Analysis of Spiro β-Lactone Proteasome Inhibitors. *J. Am. Chem. Soc.* **2008**, *130*, 14981–14983.

(36) Denora, N.; Potts, B. C. M.; Stella, V. J. A Mechanistic and Kinetic Study of the β-Lactone Hydrolysis of Salinosporamide A (NPI-0052), a Novel Proteasome Inhibitor. *J. Pharm. Sci.* **2007**, *96*, 2037–2047.

(37) Potential contributions from the neighboring carboxylate anion are unknown.

(38) Cassidy, C. S.; Lin, J.; Frey, P. A. A New Concept for the Mechanism of Action of Chymotrypsin: The Role of the Low-Barrier Hydrogen Bond. *Biochemistry* **1997**, *36*, 4576–4584.

(39) Lin, J.; Cassidy, C. S.; Frey, P. A. Correlations of the Basicity of His 57 with Transition State Analogue Binding, Substrate Reactivity, and the Strength of the Low-Barrier Hydrogen Bond in Chymotrypsin. *Biochemistry* **1998**, *37*, 11940–11948.
(40) Lin, J.; Westler, W. M.; Cleland, W. W.; Markley, J. L.; Frey, P. A. Fractionation Factors and Activation Energies for Exchange of the Low Barrier Hydrogen Bonding Proton in Peptidyl Trifluoromethyl Ketone Complexes of Chymotrypsin. *Proc. Natl. Acad. Sci. U.S.A.* **1998**, *95*, 14644–14668.
(41) Tanford, C. The Interpretation of Hydrogen Ion Titration Curves of Proteins. *Adv. Protein Chem.* **1962**, *17*, 69–165.
(42) Hale, R.; Miller, C.; Manam, R. R.; Macherla, V. R.; Palladino, M.; Potts, B.; Chandra, J. Analysis of Reactive Oxygen Species (ROS) Generation and Caspase-8 Activation by Analogs of Proteasome Inhibitor NPI-0052. In *Proceedings of the 100th Annual Meeting of the American Association for Cancer Research*, Denver, CO, Apr 18−22, 2009; AACR: Abstract 5634.
(43) Reed, K. A.; Manam, R. R.; Mitchell, S. S.; Xu, J; Teisan, S.; Chao, T.-H.; Deyanat-Yazdi, G.; Neuteboom, S. T. C.; Lam, K. S.; Potts, B. C. M. Salinosporamides D−J from the Marine Actinomycete Salinispora tropica, Bromosalinosporamide, and Thioester Derivatives Are Potent Inhibitors of the 20S proteasome. *J. Nat. Prod.* **2007**, *70*, 269–276.
(44) Groll, M.; Huber, R. Purification, Crystallization and X-ray Analysis of the Yeast 20S Proteasomes. *Methods Enzymol.* **2005**, *398*, 329–336.
(45) Kabsch, W. Automatic Processing of Rotation Diffraction Data from Crystals of Initially Unknown Symmetry and Cell Constants. *J. Appl. Crystallogr.* **1993**, *26*, 795–800.